The Ambient Hydration of the Aluminophosphate JDF-2 to AlPO-53(A): Insights from NMR Crystallography

Authors

Daniel M. Dawson[a]*, Richard I. Walton[b], Stephen Wimperis[c] and Sharon E. Ashbrook[a]*

[a]School of Chemistry, Centre for Magnetic Resonance and EaStCHEM, University of St Andrews, North Haugh, St Andrews, Fife, KY16 9ST, UK

[b]Department of Chemistry, University of Warwick, Gibbet Hill Road, Coventry, CV4 7AL, UK

[c]Department of Chemistry, Lancaster University, Lancaster, LA1 4YB, UK

Correspondence email: dmd7@st-andrews.ac.uk; sema@st-andrews.ac.uk

Synopsis Using multinuclear solid-state NMR spectroscopy and first-principles DFT calculations, we examine the slow ambient hydration of the AEN-type aluminophosphate, JDF-2, to AlPO-53(A). We propose a modified version of the published structure of AlPO-53(A), with reorientation of the methylammonium cations and partial occupancy of the water sites.

Abstract The aluminophosphate (AlPO), JDF-2 is prepared hydrothermally with methylammonium hydroxide (MAH^+ HO^-, $MAH^+ = CH_3NH_3^+$), giving rise to a microporous AEN-type framework with occluded MAH^+ and extraframework (Al-bound) HO^-. Despite the presence of these species within its pores, JDF-2 can hydrate upon exposure to atmospheric moisture to give AlPO-53(A), an isostructural material whose crystal structure contains one molecule of H_2O per formula unit. This hydration can be reversed by mild heating (such as the frictional heating from magic angle spinning). Previous work has shown good agreement between NMR parameters obtained experimentally and calculated from the (optimised) crystal structure of JDF-2. However, several discrepancies are apparent between the experimental NMR parameters for AlPO-53(A) and those calculated from the (optimised) crystal structure (*e.g.*, four ^{13}C resonances are observed, rather than the expected two). The unexpected resonances appear and disappear reversibly with the respective addition and removal of H_2O, so clearly arise from AlPO-53(A). We investigate the ambient hydration of JDF-2 using quantitative ^{31}P MAS NMR to follow the transformation over the course of ~3 months. The structures of JDF-2 and AlPO-53(A) are also investigated using a combination of multinuclear solid-state NMR spectroscopy to characterise the samples, and first-principles density functional theory (DFT) calculations to evaluate a range of possible structural models in terms of calculated NMR parameters and energetics. The published structure of JDF-2 is shown to be a good representation of the dehydrated material, but modification of the published structure of AlPO-53(A) is required to provide calculated NMR

parameters that are in better agreement with experiment. This modification includes reorientation of all MAH^+ cations and partial occupancy of the H_2O sites.

Keywords: Aluminophosphate; AEN framework; zeolites; microporous materials.

1. Introduction

Microporous aluminophosphate molecular sieves (AlPOs) and their metal- and silicon-substituted analogues (MeAPOs and SAPOs, respectively) are of great interest in industry, medicine and the environment, owing to the number of zeotypic frameworks accessible by these materials and (through iso- or aliovalent substitution) their versatile chemistry.(Wilson *et al.*, 1982, Wright, 2008) During synthesis of AlPOs, the Al and P sources are combined with the required structure-directing agent (SDA) or "template" – typically an organic ammonium-based species and, in some cases, a mineraliser (*e.g.*, HF). The role of the SDA is to direct the crystallisation of the $AlPO_4$ framework, giving the desired framework connectivity, although the precise mechanism by which this occurs is not generally well understood. The material crystallises as a network of corner-sharing AlO_4 and PO_4 tetrahedra (with strict alternation of Al and P). Voids in the network (pores and channels) are typically occupied by the cationic SDA and, in many cases, occluded water molecules. As the $AlPO_4$ framework has an overall neutral charge, the positive charge of the SDA is balanced by anionic species (HO^- and/or F^-), which bind to the framework, forming five- or six-coordinate Al in addition to the four-coordinate species of the neutral framework. In many cases, the exact locations of the SDA, extra-framework anions and any water molecules present are poorly defined in reported crystal structures, owing to factors such as orientational or motional disorder of the SDA and/or H_2O, and mixed or fractional anion occupancies.(Antonijevic *et al.*, 2006, Ashbrook *et al.*, 2009, Martineau *et al.*, 2011) Given the insensitivity of Bragg diffraction techniques to these features, solid-state NMR is often used as a complementary characterisation method, owing to its sensitivity to structure on the local scale (rather than the bulk crystal scale) and dynamics occurring on timescales spanning ~12 orders of magnitude.(Ashbrook *et.al.*, 2014)

Owing to the different structural features observable by solid-state NMR and Bragg diffraction, it is unsurprising that combining results from the two techniques is often challenging, particularly when assigning the resonances observed in NMR spectra to the atomic sites present in the crystal structure. In recent years, periodic first-principles density functional theory (DFT) calculations have greatly eased this task and, consequently, gained great popularity.(Charpentier, 2011, Bonhomme *et al.*, 2012, Ashbrook and Dawson, 2014, Ashbrook and McKay, 2016) Often the excellent agreement between calculated and experimental NMR parameters enables immediate assignment and, in cases where discrepancies are apparent, these can often be explained by more detailed investigation (often by DFT and NMR spectroscopy) of the dynamics and disorder present.(Ashbrook and McKay, 2016) One of

the key advantages of DFT calculations is the ease with which the structural model can be manipulated, allowing the validation of many possible models with respect to experimental observables (*e.g.*, NMR parameters). However, care must be taken in obtaining the atomic positions in the structural models to be investigated. While these are typically based on structures obtained by Bragg diffraction, any changes to the diffraction-based structure must initially be made either manually, based on "chemical intuition", idealised bond geometries, and, ultimately, (educated) guesswork, or automatically, based on random structure generation (*e.g.*, in the *ab initio* random structure searching (AIRSS) approach of Pickard and Needs (2006)). It is, therefore, common to optimise such structural models, such that the forces acting on the atoms are minimised to within a reasonable tolerance, leading to minimum-energy structures. In addition to providing more reliable structures for the calculation of NMR parameters, the calculated energies of the optimised structures may allow an evaluation of the likelihood of such structures occurring in reality.(Ashbrook and McKay, 2016)

Common periodic planewave pseudopotential DFT methods often unrealistically expand the unit cell by *ca.* 10%, owing to an inherently poor description of the long-range electron-electron correlations (*i.e.*, van der Waals' and other "dispersion" interactions). When optimising the published crystal structure, this expansion can be overcome by constraining the unit cell parameters to those determined (generally with a high precision) by Bragg diffraction experiments. However, when modifications are made to this starting structure, the unit cell parameters must also be varied, *i.e.*, the structure is no longer that for which the average unit cell parameters were determined and such constraints are not, therefore, necessarily realistic. Recently, schemes correcting for the underestimation of dispersion forces have been introduced to periodic planewave DFT codes,(Grimme, 2006, Tkatchenko and Scheffler, 2009, McNellis *et al.*, 2009) allowing for the variation of unit cell parameters without the artificial expansion otherwise observed. Sneddon *et al.* (2014) recently showed that such semi-empirical dispersion correction (SEDC) schemes provided a means of optimising the structures of AlPOs without constraining the unit cell parameters. The resulting calculated unit cell parameters were typically in better agreement with the experimentally-determined values, while the NMR parameters obtained from the optimised structures were in much better agreement with the experimental parameters than those calculated from the initial structures. Therefore, it appears that such SEDC schemes present the best current approach for determining the minimum-energy configuration of any structural models for disorder in AlPOs, whilst imposing the minimum number of constraints on the calculation. This is an important consideration when the structures to be calculated are theoretical models that include defects or disorder, for which experimental unit cell data will represent only a bulk average, rather than accurately describing the cell containing the defect.

JDF-2 has the formula $Al_3P_3O_{12}(CH_3NH_3OH)$.(Chippindale *et al.*, 1994, Gai-Boyes, 1992) Its structure comprises an $AlPO_4$ framework with the AEN topology, with HO^- bridging Al1 and Al2

(which are, consequently, five-coordinate) and methylammonium (MAH^+) located within the two-dimensional network of pores. Despite the presence of the MAH^+, JDF-2 can hydrate reversibly under ambient conditions,(Ashbrook *et al.*, 2009) giving the isostructural AlPO-53(A), with formula $Al_6P_6O_{24}(CH_3NH_3OH)_2(H_2O)_2$, where the presence of H_2O causes a lowering of the crystallographic symmetry (from *Pbca* to $P2_12_12_1$), giving rise to six crystallographically-distinct Al and P species, two inequivalent MAH^+ and HO^- species, and two inequivalent H_2O molecules.(Kirchner *et al.*, 2000) The crystal structures of JDF-2 and AlPO-53(A) are shown in Figure 1, with the crystallographically-distinct Al, P, MAH^+, HO^- and H_2O species identified. Reports of such hydration are relatively uncommon for as-prepared AlPOs, whose pores are already occupied by guest species, and its occurrence in this case warrants further investigation, (i) in order to understand why both JDF-2 and AlPO-53(A) are stable, and (ii) as a model for the interaction of guest species in the confined spaces present in microporous materials. Ashbrook *et al.* (2009) previously observed that the hydration was facile, but relatively slow (on the timescale of weeks) under ambient conditions. In this work, a more detailed investigation of the hydration process is reported, using quantitative ^{31}P magic-angle spinning (MAS) NMR spectroscopy to follow the transformation of JDF-2 to AlPO-53(A) under ambient conditions. The discrepancy between the observed and expected number of resonances in the NMR spectra (particularly ^{13}C, as noted earlier by Ashbrook *et al.*,(2009) and ^{15}N) is also investigated using a combination of high-resolution multinuclear solid-state NMR and first-principles DFT calculations. A number of possible models for defects within AlPO-53(A), based around MAH^+ reorientations and/or H_2O vacancies are considered, with the ultimate conclusion that all MAH^+ cations must be reoriented and the H_2O partially occupied in order to provide a structure consistent with other observations.

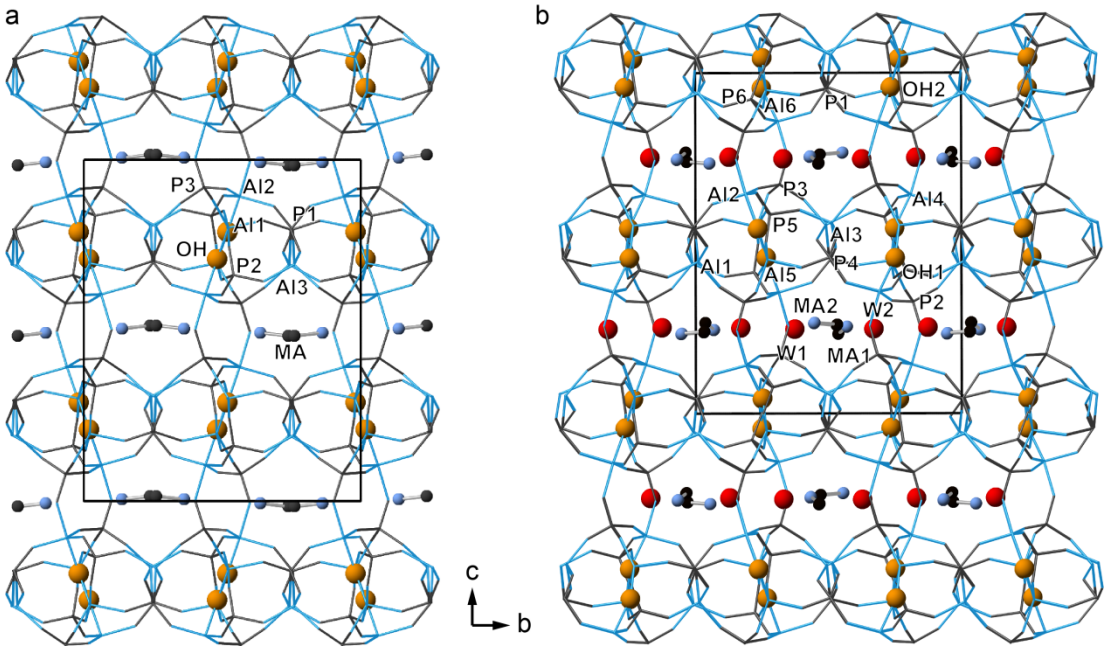

Figure 1 Crystal structures of (a) JDF-2 (Chippindale *et al.*, 1994) and (b) AlPO-53(A) (Kirchner *et al.*, 2000). The solid lines indicate the unit cell, crystallographically distinct Al (blue sticks), P (dark grey sticks), MAH^+ (blue and grey spheres) OH^- (orange spheres) and H_2O (red spheres) are indicated and H atoms are omitted for clarity.

2. Experimental

2.1. Synthesis

The samples studied in the present work are the same as those prepared for the earlier work of Ashbrook *et al.*, (2009) who reported the full synthetic procedure, based on that of Kirchner *et al.* (2000). Samples of AlPO-53(A) were dehydrated at 110 °C for between 16 and 72 h to afford JDF-2, and samples of JDF-2 were hydrated under ambient conditions or by immersion in distilled water to afford AlPO-53(A). The sample used in the ambient hydration study was stored in a sample vial covered with punctured sealing film (to minimise contamination by dust particles, *etc.*) between NMR experiments. The room temperature and relative humidity were recorded using an ETI Therma-hydrometer, and had ranges of 18.8-19.2 °C and 20-46%, respectively.

2.2. Solid-state NMR spectroscopy

Solid-state NMR spectra were recorded using Bruker Avance III spectrometers equipped with 9.4 or 14.1 T wide-bore superconducting magnets. For ^{1}H NMR spectra, samples were packed into 1.3 mm zirconia rotors and rotated at a MAS rate of 60 kHz. ^{1}H MAS NMR spectra were acquired with signal averaging for 8 transients with a repeat interval of 3 s. Two-dimensional ^{1}H homonuclear double-quantum (DQ) MAS correlation experiments were carried out with one rotor period of BABA pulses (Sommer *et al.*, 1995, Feike *et al.*, 1996) used to excite and reconvert double-quantum coherences. Signal averaging was carried out over 16 transients for each of 300 t_1 increments of 33.33 μs.

For ^{31}P, ^{27}Al and ^{13}C NMR spectra, the samples were packed into 4 mm zirconia rotors and rotated at a MAS rate of 8-12.5 kHz. ^{13}C NMR spectra were recorded with cross polarisation (CP) from ^{1}H. A spin lock of 1 ms was used, with a ramped pulse (90-100%) applied to ^{1}H. The room-temperature spectra of JDF-2 and AlPO-53(A) were recorded with signal averaging for 512 transients with a repeat interval of 3 s. The variable-temperature ^{13}C NMR spectra of AlPO-53(A) were recorded with a 1 ms spin lock, 3 s repeat interval and signal averaging for 2048 transients. The sample temperature was controlled using a Bruker BCU-II chiller and Bruker BVT/BVTB-3000 temperature controller and heater booster. The sample temperature (including frictional heating effects arising from sample spinning) was calibrated using the isotropic ^{87}Rb shift of solid RbCl.(Skibsted and Jakobsen, 1999) For all ^{13}C spectra, high-power (ν_1 = 100 kHz) TPPM-15 ^{1}H decoupling was applied during acquisition. The ^{1}H-^{13}C correlation spectrum of AlPO-53(A) was recorded using a through-bond J-transferred refocused INEPT pulse sequence.(Elena *et al.*, 2005) Signal averaging was carried out for

224 transients for each of 80 t_1 increments of 63 μs. Homonuclear decoupling of ^{1}H during t_1 was achieved using the eDUMBO-1_{22} scheme,(Elena *et al.*, 2004) and heteronuclear decoupling of ^{1}H during acquisition was achieved using TPPM-15. ^{27}Al MAS NMR spectra were recorded with signal averaging for 32 transients with a repeat interval of 5 s. The ^{27}Al multiple-quantum (MQ) MAS NMR spectrum of JDF-2 was recorded using a shifted-echo split-t_1 pulse sequence,(Brown and Wimperis, 1997) with the signal enhanced using a SPAM composite conversion pulse.(Gan and Kwak, 2004) Signal averaging was carried out for 288 transients with a 1 s repeat interval for each of 120 t_1 increments of 142.8 μs. The delay used to allow acquisition of a whole echo was 6.5 ms. The indirect dimension was referenced according to Pike *et al*. (2000). The ^{27}Al MQMAS NMR spectrum of AlPO-53(A) was recorded using a z-filtered pulse sequence, and then sheared and reference according to Pike *et al*. (2000). Signal averaging was carried out for 192 transients with a repeat interval of 1.5 s for each of 144 t_1 increments of 71.43 μs. ^{31}P MAS NMR spectra were recorded with signal averaging for 2 transients with a repeat interval of 1200 s.

For ^{15}N NMR spectra, samples were packed into 7 mm zirconia rotors and rotated at a MAS rate of 5 kHz. The spectra were recorded with cross polarisation (CP) from ^{1}H. A spin lock of 3 ms was used, with a ramped pulse (90-100%) applied to ^{1}H. The spectrum was recorded with signal averaging for 29696 transients with a repeat interval of 3 s (AlPO-53(A)) or 1600 transients with a repeat interval of 90 s (JDF-2). TPPM-15 ^{1}H decoupling (ν_1 ~45 kHz) was applied during acquisition. Note that the ^{15}N resonances for both materials are very sharp (< 14 Hz) and, therefore, the FIDs were truncated at 61 ms to prevent probe arcing. In order to minimise truncation artefacts while retaining the relevant spectral features, the FIDs were processed with 5 Hz (JDF-2) or 2.5 Hz (AlPO-53(A)) exponential weighting.

Chemical shifts are reported in ppm relative to $(CH_3)_4Si$ (^{1}H and ^{13}C), CH_3NO_2 (^{15}N), 1 M $Al(NO_3)_3$ or 85% H_3PO_4 using L-alanine ($N\mathbf{H}_3$ δ_{iso} = 8.5 ppm, $\mathbf{C}H_3$ δ_{iso} = 20.5 ppm), ^{15}N-enriched glycine (δ_{iso} = –347.4 ppm), $Al(acac)_3$ (δ_{iso} = 0.0 ppm, C_Q = 3.0 MHz, η_Q = 0.17) and BPO_4 (δ_{iso} = –29.6 ppm) as secondary solid references.

2.3. Computational details

Geometry optimisations and calculation of NMR parameters were carried out using the CASTEP DFT code (versions 8 and 16),(Clark *et al.*, 2005) employing the GIPAW algorithm,(Pickard and Mauri, 2001) to reconstruct the all-electron wavefunction in the presence of a magnetic field. The initial crystal structures were taken from the literature, and additional models were constructed from these as discussed below. Calculations were performed using the GGA PBE functional, with core-valence interactions described by ultrasoft pseudopotentials.(Yates *et al.*, 2007) A planewave energy cut off of 60 Ry was used, and integrals over the Brillouin zone were performed using a Monkhurst-Pack grid with a k-point spacing of 0.04 2π Å^{-1}. Dispersive interactions were reintroduced using the scheme of

Grimme (2006), as implemented by McNellis *et al.*(2009). Calculations were performed on either a 198-node (2376-core) Intel Westmere cluster with 2 GB memory per core and QDR Infiniband interconnects, or a 54-node (1728-core) Intel Broadwell cluster with 4 GB memory per core and FDR Infiniband interconnects at the University of St Andrews.

The calculated isotropic magnetic shielding, σ_{iso}^{calc}, was converted to a calculated isotropic chemical shift using the relationship

$$\delta_{iso}^{calc} \approx \frac{\sigma_{ref} - \sigma_{iso}^{calc}}{m} \quad , \qquad (1)$$

where σ_{ref} and m are the reference shielding and scaling factor, respectively, for a given nucleus. Ideally, m = 1, but it is sometimes the case that, in reality, non-unity scaling factors are required.(Ashbrook and McKay, 2016) The values used in this work are summarised in Table 1. The magnitude of the quadrupolar coupling constant is given by $C_Q = eQV_{ZZ}/h$, where Q is the nuclear quadrupole moment (for which a value of 146.6 mb was used for ^{27}Al).(Pyykko, 2008) The asymmetry parameter is given by $\eta_Q = (V_{XX} - V_{YY})/V_{ZZ}$.

Table 1 Reference shieldings, σ_{ref}, and scaling factors, m, used to convert calculated isotropic shieldings to isotropic chemical shifts as described in Equation 1.

Nucleus	σ_{ref} (ppm)	m	Nucleus	σ_{ref} (ppm)	m
^{1}H	27.53	0.90	^{27}Al	554.40	0.94
^{13}C	173.94	1.00	^{31}P	281.31	1.14
^{15}N	–155.60	1.00			

3. Results and Discussion

3.1. The ambient hydration of JDF-2 to AlPO-53(A)

The transformation from JDF-2 to AlPO-53(A) was followed by quantitative ^{31}P MAS NMR spectroscopy (*i.e.*, ensuring full relaxation before repeating the experiment). Using the spectral assignments reported previously,(Ashbrook *et al.*, 2009) the integrated intensities of the resonances can be used to determine the proportions of JDF-2 to AlPO-53(A) within the sample. It is important to note that at no point in the investigation were any resonances observed that did not correspond to either JDF-2 or AlPO-53(A), suggesting that, upon contact with H_2O, the transformation of one unit cell of JDF-2 to AlPO-53(A) occurs directly and not *via* any intermediate phase. The limiting factor for the overall bulk transformation must, therefore, be a combination of the availability of atmospheric water, and the transport of water through the pores of the material. Consequently, the

composition of the sample may be expressed in terms of the degree of transformation, α(t),(Boldyreva and Boldyrev, 1999)

$$\alpha(t) = 1 - \phi_{JDF\text{-}2}(t) \quad , \qquad (2)$$

where $\phi_{JDF\text{-}2}(t)$ is the fraction of the sample that remains as JDF-2 at time, t, after the start of the hydration. The degree of transformation can also be expressed as the proportion of the sample that has been converted to AlPO-53(A) after a time, t. A plot of α(t) against t is shown in Figure 2, along with the ^{31}P MAS NMR spectra used to determine α(t). The error bars indicate the standard deviation of values of α(t) determined from the integrated intensities of different spectral resonances, as described in the Supporting Information (S1).

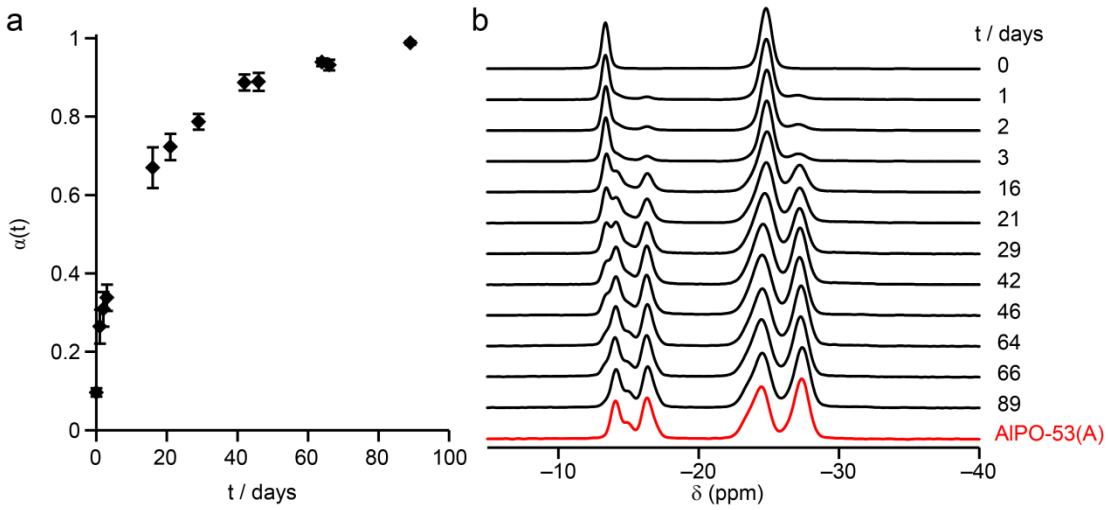

Figure 2 (a) Plot of the degree of transformation α(t) for JDF-2 to AlPO-53(A) as a function of time. Error bars indicate the standard deviation in α, obtained as described in the Supporting Information (S1). (b) ^{31}P (14.1 T, 12.5 kHz MAS) NMR spectra of JDF-2 exposed to ambient conditions for the time indicated. The ^{31}P NMR spectrum of a sample prepared as AlPO-53(A), acquired under the same conditions, is shown in red.

The data fit well to a first-order kinetic model,

$$\alpha(t) = e^{-kt} \quad , \qquad (3)$$

where k is the first-order rate constant and α(t) describes the degree of hydration of the material,

$$\alpha(t) = 1 - \frac{\phi_J(t)}{\phi_J(0)} \quad , \qquad (4)$$

with $\phi_J(t)$ representing the fraction of the material that remains as JDF-2 at time t. However, the straight-line form of the model, $-\ln(1-\alpha) = -\ln(1-\alpha_0) + kt$ has an intercept of 0.2645, indicating an initial rapid hydration of *ca.* 23% of the material within the first day. It can be assumed that this

represents hydration of the surface layers of the crystallites, with further diffusion of water into the cores of the crystallites proceeding with a rate constant, k, of 1.8×10^{-3} h^{-1}. This value is clearly much slower than the "overnight" hydration typically observed for many calcined AlPOs (see the Supporting Information (S2) for examples). However, to our knowledge, there are no other studies on the ambient hydration of as-prepared AlPOs for direct comparison, so we are unable to say with certainty whether the hydration of as-made JDF-2 is unusually rapid. Further kinetic analysis was not carried out as, although the room temperature was maintained at 19(1) °C, the relative humidity varied between 23 and 43%, depending on fluctuations in the weather.

3.2. Multinuclear solid-state NMR spectra of AlPO-53(A)

While it was noted above that no intermediate species were observed in the transformation of JDF-2 to AlPO-53(A), several resonances in the multinuclear NMR spectra of AlPO-53(A) cannot immediately be assigned to species in the published crystal structure.(Kirchner *et al.*, 2000) This was first noted by Ashbrook *et al.*,(2009) who reported four resonances in the ^{13}C NMR spectrum of AlPO-53(A), despite the structure containing only two crystallographically-distinct C sites. Here, we investigate this discrepancy further using multinuclear one- and two-dimensional NMR spectra to gain insight into the origins of the unexpected resonances.

The ^{1}H MAS NMR spectra shown in Figure 3(a) contain the expected number of resonances, according to the published crystal structures. The use of 60 kHz MAS and a repeat interval of 3 s affords high-resolution quantitative spectra. The chemical shifts, integrated intensities and assignments of all ^{1}H resonances observed for JDF-2 and AlPO-53(A) provided in Table 2. As shown in the Supporting Information (S3), two-dimensional ^{1}H double-quantum (DQ) MAS experiments confirm all assignments. From both spectra, it can be seen that the relative proportions of C**H**$_3$ and N**H**$_x$ is 1 : 1, confirming that only protonated methylammonium (MAH^+) is present in both materials. However, the relative intensity of the **H**$_2$O resonance indicates a stoichiometry closer to $Al_6P_6O_{24}(CH_3NH_3OH)_2(H_2O)_{0.5}$, *i.e.*, with only 25% occupancy of each of the two H_2O sites. This differs significantly from the thermogravimetric analysis reported by Ashbrook *et al*. (2009), which indicated that the H_2O sites were fully occupied (for a freshly-prepared sample of AlPO-53(A) dried under air at 30 °C). However, the variable hydration state of the material and the frictional heating of the sample in MAS experiments (especially 60 kHz MAS) is likely responsible for this discrepancy, especially as any surface bound water is likely to be easily removed with only gentle heating, and we note that the NMR spectra recorded for this work are consistent with those recorded earlier.(Ashbrook *et al*., (2009))

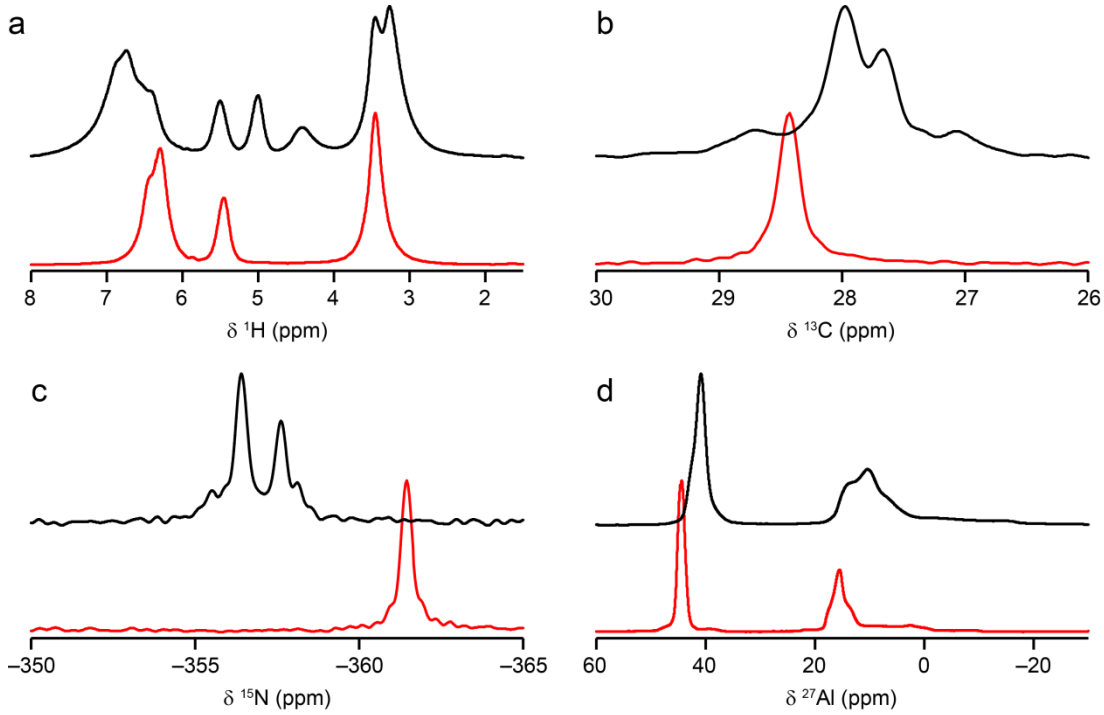

Figure 3 (a) ^{1}H (14.1 T, 60 kHz MAS), (b) ^{13}C (14.1 T, 12.5 kHz CP MAS), (c) ^{15}N (9.4 T, 5 kHz CP MAS) and (d) ^{27}Al (14.1 T, 12.5 kHz MAS) NMR spectra of (black) AlPO-53(A) and (red) JDF-2.

Table 2 Chemical shifts and relative integrated intensities of resonances observed in the ^{1}H NMR spectra of AlPO-53(A) and JDF-2.

Species	δ_{iso} (ppm)	relative intensity	Species	δ_{iso} (ppm)	relative intensity
JDF-2			AlPO-53(A)		
C**H**$_3$	3.1	3.0	C**H**$_3$	2.9, 3.1	6.0[a]
O**H**	5.3	1.1	**H**$_2$O	4.1	1.1
N**H**$_3$	6.16, 6.34	3.1[a]	O**H**	4.8, 5.3	1.2, 1.1
			N**H**$_3$	6.3–6.8	5.9[a]

a. Accurate decomposition was not possible and only the combined integrated intensity for these resonances is reported.

The ^{13}C CP MAS NMR spectrum of JDF-2 in Figure 3(b) contains a single sharp resonance at 28.5 ppm, as expected from the single crystallographic MAH^{+}. However, as previously observed by Ashbrook *et al.*,(2009) the equivalent spectrum for AlPO-53(A), also shown in Figure 3(b) contains four, rather than the expected two, resonances at 27.1, 27.7, 28.0 and 28.7 ppm. The relative intensity ratio of these four resonances is 1.0 : 2.4 : 5.3 : 1.0, which does not fit unambiguously to a simple stoichiometric ratio. However, it is worth noting that the sum of the integrated intensities of the three

least intense resonances is close to that of the most intense resonance. This suggests that one of the crystallographic MAH^+ species may be responsible for the most intense resonance, while the other three arise from the second MAH^+ species, in a range of magnetically inequivalent environments (*i.e.*, there is some non-periodic feature of the system that affects exclusively (or predominantly) one of the two crystallographic MAH^+ species within the published structure). The two-dimensional ^{1}H-^{13}C correlation spectrum shown in Figure 4 demonstrates that the ^{1}H resonance at 3.1 ppm correlates to the three ^{13}C resonances at 27.1, 27.7 and 28.0 ppm, whereas the remaining ^{13}C resonance (at 28.0 ppm) correlates to the ^{1}H resonance at 2.9 ppm. Therefore, it seems that the most likely explanation for the differences between the number of CH_3 resonances observed in the ^{1}H and ^{13}C NMR spectra is that one of the two crystallographic MAH^+ species in AlPO-53(A) is disordered, whereas the other is fully ordered. This disorder appears to give rise to a small change in the local environment of the CH_3 group, which is too small to be detected in the (relatively low-resolution) ^{1}H NMR spectrum, but yields a measurable chemical shift difference for ^{13}C.

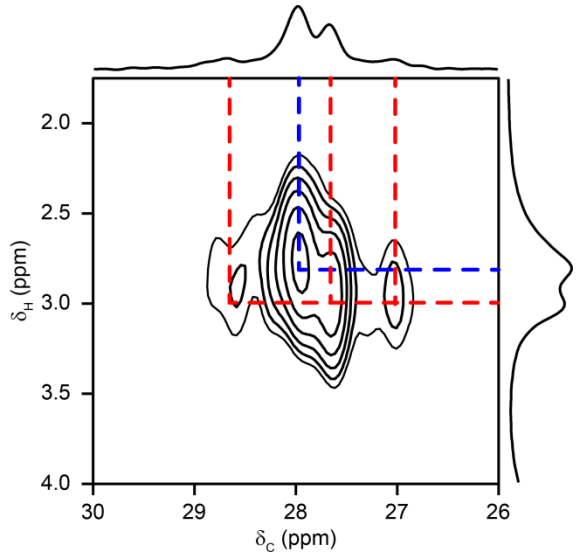

Figure 4 ^{1}H-^{13}C (14.1 T, 12.5 kHz MAS) J-transferred INEPT spectrum of AlPO-53(A).

The ^{15}N CP MAS NMR spectra of the two materials (Figure 3(c)) are similar in appearance to the ^{13}C spectra, in that a single, sharp resonance is observed for JDF-2 (δ = –361.3 ppm) and four resonances are observed for AlPO-53(A), at –356.4, –355.5, –357.6 and –358.2 ppm. This is consistent with the presence of four distinct MAH^+ species within AlPO-53(A) and the relative intensities of the ^{15}N and ^{13}C resonances are summarised in Table 3. As was indicated by the ^{1}H NMR spectra discussed above, no resonances from neutral $CH_3\mathbf{N}H_2$ are observed in the ^{15}N NMR spectra. It can, therefore, be concluded from a combination of the integrated intensities of the ^{1}H NMR spectrum and ^{15}N chemical shifts, that there are no OH^- vacancies (*i.e.*, giving rise to neutral MA) within AlPO-53(A).

Table 3 Chemical shifts and relative integrated intensities of resonances observed in the ^{13}C and ^{15}N NMR spectra of AlPO-53(A) and JDF-2.

^{13}C δ_{iso} (ppm)	relative intensity	^{15}N δ_{iso} (ppm)	relative intensity
JDF-2			
28.5	1.0	–361.3	1.0
AlPO-53(A)			
27.1	1.0	–356.4	1.0
27.7	2.4	–355.5	4.1
28.0	5.3	–357.6	2.1
28.7	1.0	–358.2	1.1

The ^{31}P MAS NMR spectrum of JDF-2, shown in Figure 2(b), contains resonances at –13.4 and –24.8 ppm, with a 1:2 integrated intensity ratio. These have been assigned previously by Ashbrook *et al.*,(2009) as summarised in Table 4. The ^{13}P MAS NMR spectrum of AlPO-53(A), shown in red in Figure 2(b) contains four intense resonances at –14.2, –16.3, –24.3 and –27.3 ppm, with approximate intensity ratios of 1 : 1 : 2 : 2. These correspond to the six crystallographically-distinct P species, as summarised in Table 4. However, as shown in Figure 5, there is also some signal intensity at –15, –19, –23 and –31 ppm, accounting for *ca.* 15% of the total spectral intensity, which cannot be assigned directly to any of the crystallographic P species. This spectral intensity disappears on dehydration of the AlPO-53(A) sample to JDF-2, and returns upon rehydration of the JDF-2 to AlPO-53(A), confirming that this signal must be assigned to AlPO-53(A), rather than an impurity phase. It should be noted that the intensity of this unassigned ^{31}P signal is similar to the sum of the integrated intensities of the two lowest-intensity resonances in both the ^{13}C and ^{15}N CP MAS NMR spectra (21 and 25%, respectively). This suggests that whatever structural modification affecting the NMR spectra of the MAH^+ species may also affect the NMR parameters of the $AlPO_4$ framework.

Table 4 Chemical shifts and assignments of the ^{31}P and ^{27}Al resonances of AlPO-53(A) and JDF-2. For ^{27}Al (spin I = 5/2), the magnitude of the quadrupolar coupling constant, $|C_Q|$, and asymmetry, η_Q, are also reported.

Assignment[a]	δ_{iso} (ppm)	$\|C_Q\|$ / MHz	η_Q
JDF-2			
P2	–13.4		

P1+P3	–24.8		
Al1	18(1)	6.6(1)	0.2(1)
Al2	18(1)	2.8(1)	0.8(1)
Al3	45(1)	1.7(1)	0.5(1)
AlPO-53(A)			
P6	–14.2		
P5	–16.3		
P1, P4	–24.3		
P2, P3	–27.3		
Al2+Al4	16(1)	4.3(2)	0.4(1)
Al5	17(1)	5.6(2)	0.9(1)
Al6	19(2)	9.7(2)	0.1(1)
Al3	42(1)	1.9(1)[b]	
Al1	44(1)	2.6(1)[b]	

a. Using the numbering schemes of Chippindale *et al.* (1994) (JDF-2) and Kirchner *et al.* (2000) (AlPO-53(A)).

b. Only the quadrupolar product, P_Q (= C_Q [1 + (η_Q^2/3)]$^{1/2}$) could be determined for these resonances. See the Supporting Information (S4) for details.

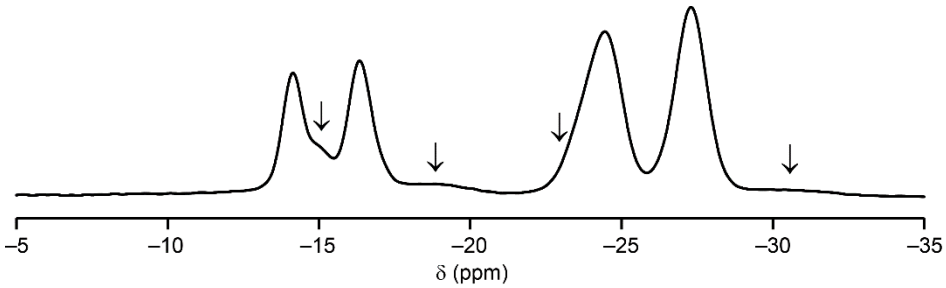

Figure 5 ^{31}P (14.1 T, 12.5 kHz MAS) NMR spectrum of as-prepared AlPO-53(A). Resonances not expected from the given crystal structure of AlPO-53(A) are indicated.

It was previously shown by Ashbrook *et al.*(2009) that the experimental ^{27}Al NMR parameters of AlPO-53(A), summarised in Table 4, are broadly consistent with those calculated from the (optimised) structure of Kirchner *et al.*, (2000), suggesting that any disorder present within AlPO-53(A) does not affect the ^{27}Al NMR parameters as significantly as those of ^{31}P. Spectra recorded for this work, shown in Figure 3(d) and the Supporting Information (S4), confirmed this observation, and the ^{27}Al MAS NMR spectrum of JDF-2 is also consistent with both the earlier work and the published crystal structure.(Chippindale *et al.*, 1994, Gai-Boyes, 1992) However, it is possible that any effects

of the disorder apparent in the NMR spectra of the other nuclei present within AlPO-53(A) are masked by the second-order quadrupolar broadening of the ^{27}Al (I = 5/2) resonances.

3.3. DFT-based investigation of the local structure of AlPO-53(A)

In the present case, it can be assumed that the $AlPO_4$ framework itself is not significantly altered upon hydration of JDF-2 to AlPO-53(A), as the hydration and dehydration processes involved occur at very low temperatures relative to the 400 °C required to calcine either material to the ordered AlPO-53(B), and even higher temperatures (*ca*. 700 °C) are required to break and reform Al-O and P-O bonds to give first AlPO-53(C) and then dense $AlPO_4$ tridymite.(Kirchner *et al.*, 2000) It is, therefore, reasonable to consider that any disorder within AlPO-53(A) must arise from the hydrated methylammonium hydroxide sublattice. As can be seen in Figure 1, the hydroxides are trapped within the "layers" of $AlPO_4$, with the methylammonium hydrate occupying the spaces between successive aluminophosphate hydroxide "layers". The hydroxide anions are, therefore, also excluded from consideration in the following discussion, since their position is essentially restricted by the surrounding $AlPO_4$ framework, which does not vary between AlPO-53(A) and JDF-2. Therefore, the methylammonium hydrate layers in the structure must contain the disorder responsible for the observed NMR spectra. This is, perhaps, unsurprising, given that this layer contains predominantly discrete molecules and ions, rather than an infinitely-connected framework, so it may be expected to have more degrees of freedom. In addition, the atoms of the methylammonium hydrate layers have low atomic numbers and will be challenging to locate by Bragg powder diffraction techniques (the original structure was determined using synchrotron powder X-ray diffraction(Kirchner *et al.*, 2000)), especially in the presence of the higher electron density of the $AlPO_4$ framework, which is generally of more interest to the materials science community, as it is this framework that will remain in the calcined material.

Within the unit cell of AlPO-53(A), there are two crystallographically-identical methylammonium hydrate layers, containing two crystallographically-distinct methylammonium species, MAH^+1 and MAH^+2, and two crystallographically-distinct water molecules, W1 and W2. As shown in Figure 6, these species are organised into $MAH^+1\cdots W2\ W1\cdots MAH^+2$ motifs, where "$\cdots$" represents the $O\cdots H$-N hydrogen bonds between the water and methylammonium. Several chemically- and physically-plausible structures can be generated from this starting point, based either on reversal of the C/N coordinates of MAH^+ (*i.e.*, assuming that the location of the MAH^+ was identified correctly by Kirchner *et al.* (2000), but its orientation was not), or on the absence of one or more water molecules (*i.e.*, assuming that the published structure of AlPO-53(A) is the idealised fully-hydrated end point of hydration of JDF-2, whereas a partially-hydrated material is the stable equilibrium state under ambient conditions).

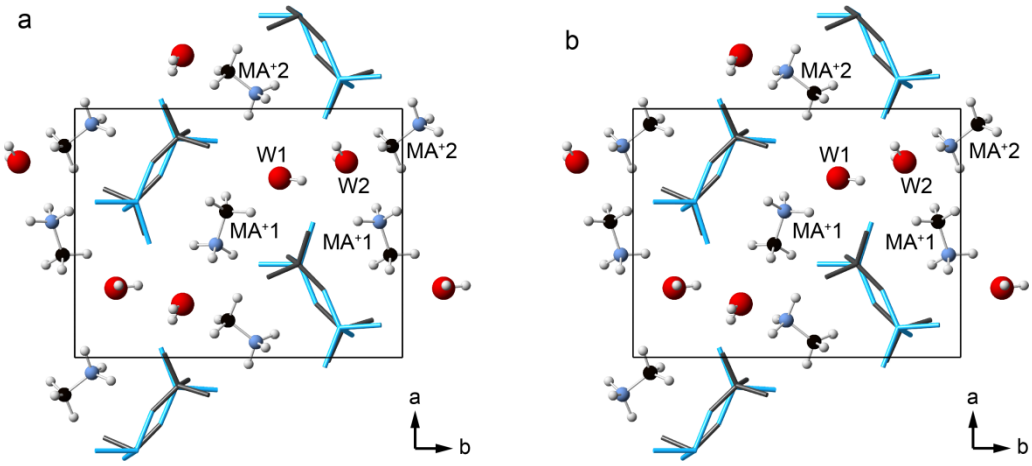

Figure 6 One of the methylammonium hydrate layers of (a) the published structure of AlPO-53(A), model A1, and (b) model A4, where the C and N of each MAH^+ have been reversed. See the text and Supporting Information (S5) for details.

The most obvious constraint on any structural models of AlPO-53(A) is that, when dehydrated, they must yield JDF-2. When optimised, JDF-2 (model J1) has a dispersion-corrected total enthalpy of –58257.298 eV, which is 0.856 eV more stable than the optimised structure of AlPO-53(A), where the water molecules have been removed prior to optimisation (model A2). However, after optimisation, a structural model of dehydrated AlPO-53(A), where the C and N coordinates were swapped (model A3), has a total enthalpy of –58257.290 eV, *i.e.*, very close to that of the optimised JDF-2. Upon optimisation, a structural model for JDF-2, in which the C and N coordinates were swapped (model J2), had a total enthalpy of –58256.335 eV, which is 0.963 eV less stable than model J1. This suggests that the orientation of the MAH^+ cations in AlPO-53(A) is the opposite of that reported by Kirchner *et al.* (2000), whereas the cation orientation in the published structure of JDF-2 (Chippindale *et al.*, 1994) is correct. Further details and all optimised structures discussed are provided in the Supporting Information (S5) and Underpinning Data.

Figure 6(b) shows the arrangement of the methylammonium hydrate layers in the structural model of AlPO-53(A) with the MAH^+ cations reversed. It can be seen that there is still potential for hydrogen bonding similar to that in the parent structure (Figure 6(a)), but now in a $MAH^+1\cdots W1\ W2\cdots MAH^+2$ motif. After optimisation, the enthalpies of the two fully-hydrated structural models (A1 and A4) shown in Figure 6 are very similar, with model A1 only 0.034 eV less stable than A4, as opposed to the 0.844 eV difference between the dehydrated models, A2 and A3. The greater similarity of the energies of the hydrated structural models likely arises from the potential to stabilise an unfavourable arrangement of cations within the pores by hydrogen bonding to H_2O, which is not possible in the dehydrated structures discussed above. However, the cation arrangement in the published structure remains energetically disfavoured relative to reversal of the cation orientations.

The quantitative ^{1}H MAS NMR spectra, discussed above, indicated that the H_2O sites were only ~25% occupied. To investigate which water site is most energetically favourable to occupy, a series of structures with W1 and W2 vacancies was considered. Removal of a single W2 (model A6) is (after optimisation) 0.040 eV more favourable than removal of a single W1 (model A5). However, for model A4, removal of W1 (model A7) is 0.379 eV more favourable than removal of W2 (model A8). When all W1 are removed from model A1 (before optimisation, model A9), this arrangement is 0.186 eV more stable than when all W2 sites are vacant (model A10), *i.e.*, 0.047 eV more stable per H_2O removed. However, when all W1 are removed from model A4 (before optimisation, model A11), this arrangement is just 0.035 eV more stable per H_2O removed, *i.e.*, around one tenth of the value observed when a single W1 is removed (model A12). This suggests that the removal of W1 from this more likely parent structure is actually less favoured as more W1 is removed. In all cases investigated, loss of W1 was energetically favoured to some extent but, in order to achieve a total of 25% occupancy of the H_2O sites, 50% of W2 sites would also have to be vacant.

The ^{13}C and ^{15}N chemical shifts calculated for models J1 and those based on A4 are plotted in Figure 7, overlaid with the experimental NMR spectra of AlPO-53(A). It can be seen that the calculated ^{13}C shifts agree best for the more dehydrated structures (*i.e.*, ^{13}C next to a water vacancy). The most intense resonance agrees well with the predicted shifts for C2 adjacent to a W1 vacancy (proposed above to be the more energetically-favourable water vacancy), which is consistent with the high relative intensity of this resonance. The resonances at 28.7 and 27.7 ppm can be assigned to C1 adjacent to a W2 vacancy, but the resonance at 27.1 ppm remains unassigned by these calculations. On the other hand, the calculated ^{15}N chemical shifts appear to indicate a much more hydrated structure, with the most intense resonance at –355.5 ppm assigned to N2 adjacent to an occupied W2 site (*i.e.*, the most energetically favourable water location). However, there is a considerably greater spread of the calculated ^{15}N shifts than was observed for ^{13}C, meaning that assignment of the other three resonances is more challenging. In general, however, from the calculated ^{13}C and ^{15}N chemical shifts, it can be concluded that the water appears to be preferentially associated with the hydrophilic NH_3^+ groups while the water vacancies are preferentially associated with the hydrophobic CH_3 groups.

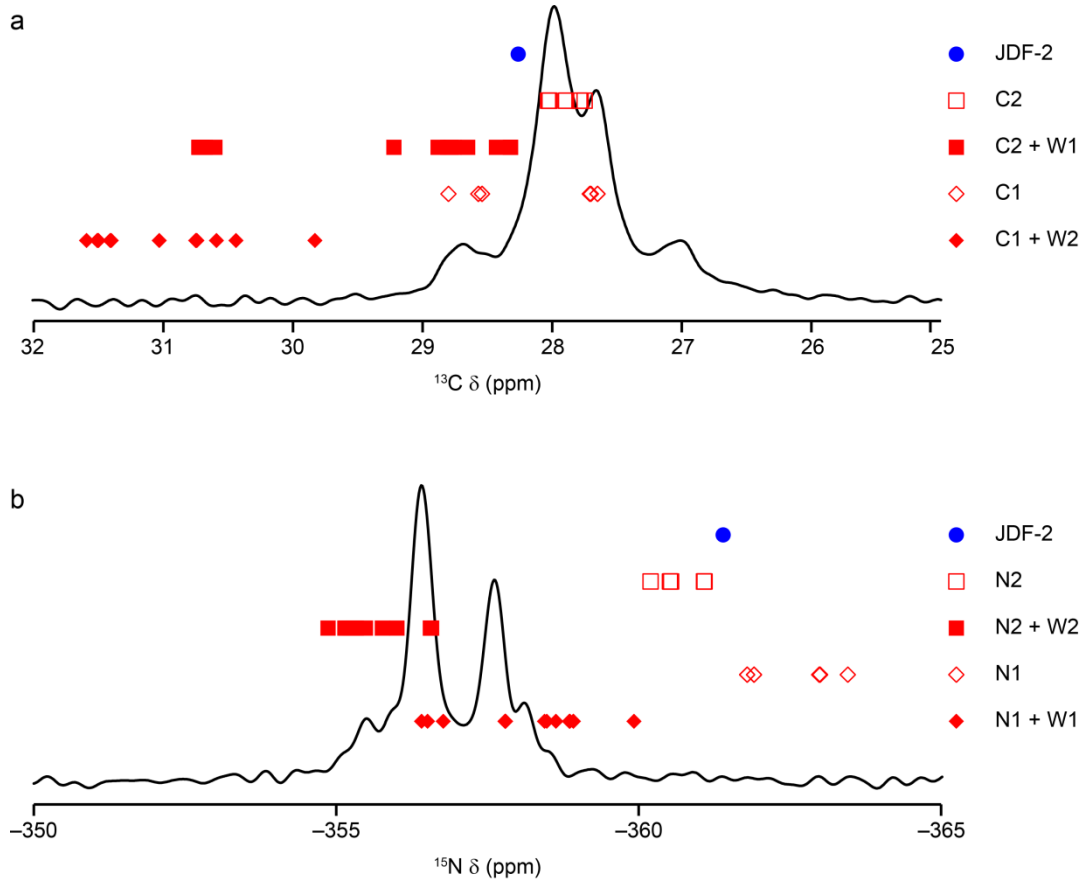

Figure 7 Experimental (a) ^{13}C and (b) ^{15}N CP MAS NMR spectra of AlPO-53(A), overlaid with the calculated isotropic chemical shifts for the different types of C and N species in the structural models J1 and those based on A4 (see the Supporting Information (S5) for details). Filled red shapes indicate that the water site (W1 or W2) adjacent to the C or N site is occupied and empty shapes indicate that the water site is vacant.

As shown in Figure 8, the ^{13}C NMR spectrum of AlPO-53(A) changes with temperature, with the peak positions and relative intensities of the resonances varying significantly between –10 to 60 °C. Such temperature dependence of the spectrum is indicative of dynamics, which means that static snapshots of possible models of disorder considered above are unlikely to provide good agreement with the experimental spectra. A full investigation of the dynamics present would require molecular-dynamics (MD) calculations and further in-depth NMR experiments such as probing variation in the ^{27}Al and ^{2}H quadrupolar broadening as a function of temperature. However, to a first approximation, assuming an almost instantaneous "hopping" motion between two structures, the calculated NMR parameters for these two structures can simply be averaged (see, for example, Griffin *et al.*, 2009). In AlPO-53(A), it is reasonable to assume that, since the water sites are only ~25% occupied, the water molecules can hop between the W1 and W2 sites with relatively little hindrance. Two calculations (models A13 and A14) were carried out with a single water molecule placed in either the W1 or W2 position of a MAH^{+}1···W2 W1···MAH^{+}2 motif and the isotropic ^{13}C and ^{15}N shifts for MAH^{+}1···□

W1···MAH$^+$2 and MAH$^+$1···W2 □···MAH$^+$2 (where □ represents a water vacancy) were averaged. This gave values of δ_{iso} for C1 and C2 of 30.0 and 29.7 ppm, and for N1 and N2 of –358.6 and –359.7 ppm. These still do not agree perfectly with the experimental spectra, but this is perhaps not surprising as the model takes into account only one type of motion and does not allow for any more complicated or longer-range water motion (which must occur as part of the hydration/dehydration process).

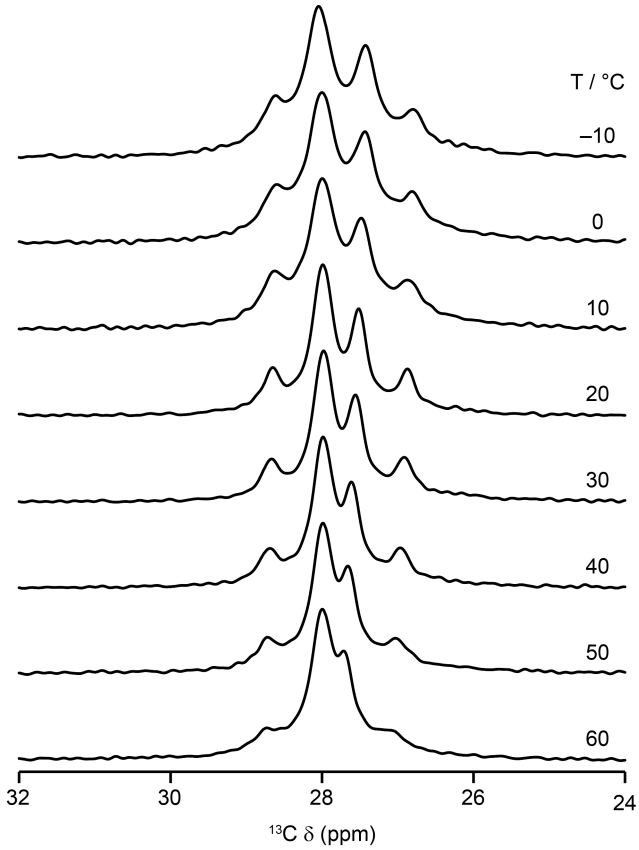

Figure 8 Variable-temperature ^{13}C (14.1 T, 12.5 kHz CP MAS) NMR spectra of AlPO-53(A).

The ^{31}P NMR spectrum of AlPO-53(A) also displayed unexpected resonances, as highlighted in Figure 5. However, as shown in the Supporting Information (S6), no one model provides agreement with the experimental shifts sufficient to allow a more detailed assignment. Again, this is not particularly surprising, as we have demonstrated the presence of dynamics, which were not included in any of the models considered for ^{31}P.

4. Conclusions

Using quantitative ^{31}P MAS NMR spectroscopy, we have demonstrated that the ambient hydration of JDF-2 to AlPO-53(A) proceeds slowly, with the hydration complete after ~3 months under the conditions employed. However, the endpoint of this hydration (when studied by solid-state NMR spectroscopy) is not consistent with the published structure of AlPO-53(A) reported by Kirchner *et al.* (2000). The structure obtained by ambient hydration is evidently significantly more disordered than refined by Kirchner *et al.*, and a combination of multinuclear solid-state NMR spectroscopy and

periodic density functional theory calculations were used to evaluate possible models for modifications to the published crystal structure. The DFT calculations suggested that reversal of the C and N positions of the MAH^+ cations was energetically favourable and gave a structure comparable to JDF-2. Quantitative ^1H MAS NMR spectra showed ~25% occupancy of the H_2O sites. However, it should be noted that the JDF-2/AlPO-53(A) system clearly has a variable hydration capacity, meaning that the published crystal structure may have been determined for a more completely hydrated material (although attempts to force the hydration to occur by submerging the material in water – results not shown – did not lead to a noticeably more hydrated material). While no one structural model considered here could adequately explain all of the spectral data, DFT calculations indicate that water vacancies on the W1 site would be most energetically favourable. Calculated ^{13}C and ^{15}N chemical shifts indicate that the more hydrophobic CH_3 end of the MAH^+ cations are, generally, near an environment closer to a water vacancy than a water molecule, whereas the water is more associated with the hydrophilic NH_3^+ group. However, variable-temperature ^{13}C NMR spectroscopy indicated that dynamics are present, probably including some bulk water motion, which is an integral part of the hydration and dehydration process.

Ultimately, we propose a model of AlPO-53(A) in which all MAH^+ cations have their C and N positions swapped compared to the crystal structure previously reported and with the overall formula $Al_6P_6O_{24}(CH_3NH_3OH)_2(H_2O)_{0.5}$. The water molecules are likely to be more closely associated with the polar NH_3^+ groups of MAH^+ than the hydrophobic CH_3 groups, but the water (and, possibly the SDA), are dynamic. These results demonstrate the power of the NMR crystallographic approach to provide structural detail beyond that available from either NMR spectroscopy or crystallography alone.

Acknowledgements The authors would like to thank EPSRC for computational support through the Collaborative Computational Project on NMR Crystallography (CCP-NC), via EP/M022501/1 and EP/J501510/1. SEA would like to thank the Royal Society and Wolfson Foundation for a merit award. We thank EaStCHEM for computational support through the EaStCHEM Research Computing Facility. The research data (and/or materials) supporting this publication can be accessed at DOI: 10.17630/bad7af52-94cc-4a85-8aed-09fb761b894c.

References

Antonijevic, S., Ashbrook, S. E., Biedasek, S., Walton, R. I., Wimperis, S. & Yang, H. (2006) *J. Am. Chem. Soc.*, **128**, 8054-8062.

Ashbrook, S. E., Cutajar, M., Griffin, J. M., Lethbridge, Z. A. D., Walton, R. I. & Wimperis, S. (2009) *J. Phys. Chem. C*, **113**, 10780-10789.

Ashbrook, S. E. & Dawson, D. M. (2013) *Acc. Chem. Res.*, **46**, 1964-1974.

Ashbrook, S. E., Dawson, D. M. & Seymour, V. R. (2014) *Phys. Chem. Chem. Phys.*, **16**, 8223-8242.

Ashbrook, S. E. & McKay, D. (2016) *Chem. Commun.*, **45**, 7186-7204.

Brown, S. P. & Wimperis, S. (1997) *J. Magn. Reson.*, **124**, 279-285.

Bonhomme, C., Gervais, C., Babonneau, F., Coelho, C., Pourpoint, F., Azaïs, T., Ashbrook, S. E., Griffin, J. M., Yates, J. R., Mauri, F. & Pickard, C. J. (2012) *Chem. Rev.*, **112**, 5733-5779.

Charpentier, T. (2011) *Solid State Nucl. Magn. Reson.*, **40**, 1-20.

Chippindale, A. M., Powell, A. V., Jones, R. H., Thomas, J. M., Cheetham, A. K., Huo, Q. & Xu, R. (1994) *Acta Cryst.*, **C50**, 1537-1540.

Clark, S. J., Segall, M. D., Pickard, C. J., Hasnip, P. J., Probert, M. J., Refson, K. & Payne, M. C. (2005) *Z. Kristallogr.*, **220**, 567-570.

Elena, B., de Paëpe, G & Emsley, L. (2004) *Chem. Phys. Lett.*, **398**, 532-538.

Elena, B., Lesage, A, Steuernagel, S., Bockmann, A. & Emsley,, L. (2005) *J. Am. Chem. Soc.*, 127, 17296-17302.

Feike, M., Demco, D. E., Graf, R., Gottwald, J., Hafner, S. & Spiess, H. W. (1996) *J. Magn. Reson. A*, **122**, 214-221.

Gan, Z. & Kwak, H. T. (2004) *J. Magn. Reson.*, **168**, 346-351.

Gai-Boyes, P. L., Thomas, J. M., Wright, P. A., Jones, R. H., Natarajan, S., Chen, J. S. & Xu, R. R. (1992) *J. Phys. Chem.*, **96**, 8206-8209.

Griffin, J. M., Wimperis, S., Berry, A. J., Pickard, C. J. & Ashbrook, S. E. (2009) *J. Phys. Chem. C* **113**, 465–471.

Grimme, S. (2006) *J. Comput. Chem.*, **27**, 1787-1799.

Kirchner, R. M., Grosse-Kunstleve, R. W., Pluth, J. J., Wilson, S. T., Broach, R. W. & Smith, J. V. (2000) *Micropor. Mesopor. Mater.*, **39**, 319-332.

Martineau, C.; Mellot-Draznieks, C. & Taulelle, F. (2011) *Phys. Chem. Chem. Phys.*, **13**, 18078-18087.

McNellis, E. R., Meyer, J. & Reuter, K. (2009) *Phys. Rev. B*, **80**, 205414.

Pickard, C. J. & Mauri, F. (2001) *Phys Rev. B*, **63**, 245101.

Pickard, C. J. & Needs, R. J. (2006) *Phys. Rev. Lett.*, **97**, 045504.

Pike, K. J., Malde, R. P., Ashbrook, S. E., McManus, J. & Wimperis, S. (2000) *Solid State Nucl. Magn. Reson.*, **16**, 203-215.

Pyykko, P. (2008) *Mol. Phys.*, **106**, 1965-1974.

Skibsted, J. & Jakobsen, H. J. (1999) *J. Phys. Chem. A*, **103**, 7958-7971

Sneddon, S., Dawson, D. M. & Ashbrook, S. E. (2014) *Phys. Chem. Chem. Phys.*, **16**, 2660-2673.

Sommer, W., Gottwald, J., Demco, D. E. & Spiess, H. W. (1995) *J. Magn. Reson. A*, **113**, 131–134.

Tkatchenko, A. & Scheffler, M. (2009) *Phys. Rev. Lett.*, **120**, 073005.

Wilson, S. T., Lok, B. M., Messina, C. A., Cannan, T. R. & Flanigen, E. M. (1982) *J. Am. Chem. Soc.*, **104**, 1146-1147.

Wright, P. A. (2008) *Microporous Framework Solids*, 1st edn., The Royal Society of Chemistry, Cambridge, UK.

Yates, J. R., Pickard, C. J. & Mauri, F. (2007) *Phys. Rev. B*, **76**, 024401.

Supporting information

S1. Approximate Errors in α(t)

Considering the ^{31}P MAS NMR spectrum of a mixture of JDF-2 and AlPO-53(A) of composition ϕ_J JDF-2 + ϕ_A AlPO-53(A), where $\phi_J + \phi_A = 1$ (and, hence, $\phi_A = \alpha(t)$), the spectrum can be separated into four distinct regions as shown in Figure S1. Region W (–12.0 to –15.5 ppm) has intensity I_W and contains resonances from P2 of JDF-2 and P6 of AlPO-53(A). Region X (–15.5 to –20.0 ppm) has intensity I_X and contains only the P5 resonance of AlPO-53(A). Region Y (–22 to –25.8 ppm) has intensity I_Y, and contains resonances from P1 and P3 of JDF-2 and P1 and P4 of AlPO-53(A). Region Z (–25.8 to –35 ppm) has intensity I_Z and contains the P2 and P3 resonances of AlPO-53(A). Using the notation I_{nM}, where n = the crystallographic P species and M = J or A (denoting JDF-2 or AlPO-53(A), respectively), the intensities of the regions are

$$I_W = I_{2J} + I_{6A} \quad , \tag{S1}$$

$$I_X = I_{5A} \quad , \tag{S2}$$

$$I_Y = I_{1J} + I_{3J} + I_{1A} + I_{4A} \quad , \tag{S3}$$

and

$$I_Z = I_{2A} + I_{3A} \quad . \tag{S4}$$

Given that all P species have equal occupancy in the crystal structures of JDF-2 and AlPO-53(A), and expressing I_W, I_X, I_Y and I_Z as a fraction of the total spectral intensity, Equations S1-S4 can be rewritten in terms of α(t), giving theoretical intensities of

$$I_w = \frac{1}{3}\left(1 - \frac{\alpha(t)}{2}\right) \quad , \tag{S5}$$

$$I_X = \frac{\alpha(t)}{6} \quad , \tag{S6}$$

$$I_Y = \frac{2}{3}\left(1 - \frac{\alpha(t)}{2}\right) \quad , \tag{S7}$$

and

$$I_Z = \frac{\alpha(t)}{3} \quad . \tag{S8}$$

The value of α(t) can, therefore, be determined by integration of the quantitative ^{31}P MAS NMR spectrum (including first-order SSBs) of a sample of JDF-2 exposed to ambient moisture for a given

time period. The intensities of all four regions can be obtained from one spectrum, allowing four values of $\alpha(t)$ to be determined and providing some indication of the error associated with this approach. Values plotted in Figure 2(a) of the main text represent the mean value of $\alpha(t)$, with the error bars representing the standard deviation of the values obtained from each of the four regions.

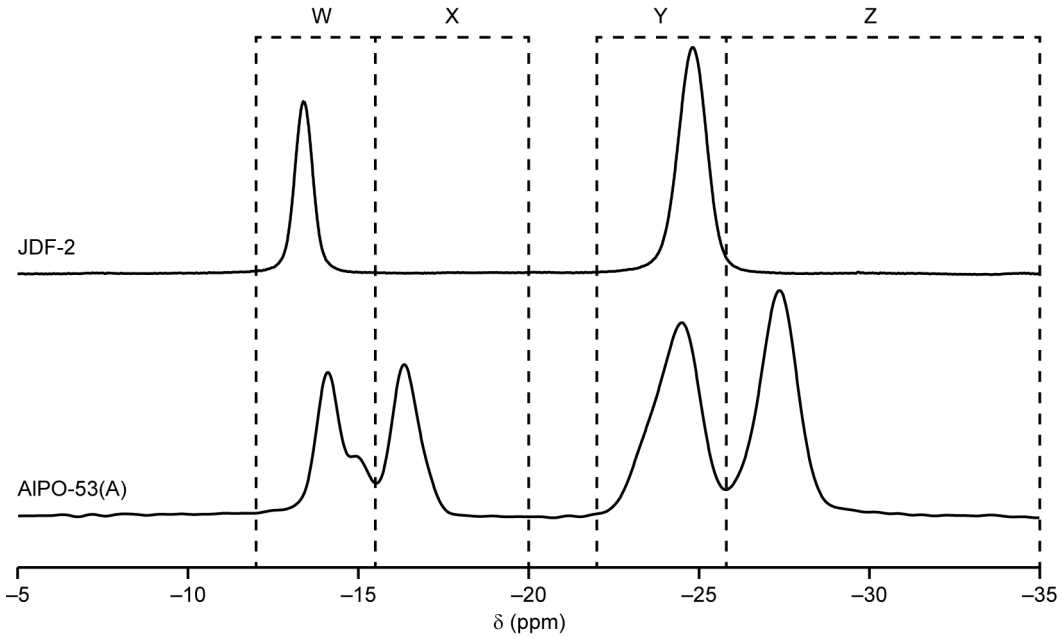

Figure S1 ^{31}P (14.1 T, 12.5 kHz MAS) NMR spectra of JDF-2 and AlPO-53(A). The regions used to determine $\alpha(t)$ are indicated.

S2. Ambient Hydration of Calcined AlPO-53(B)

Figure S2 shows the evolution of the ^{31}P NMR spectra of the calcined AlPOs, AlPO-53(B) (AEN type), and AlPO-34 (CHA type), as a function of time exposed to ambient moisture. It can be seen that the materials reaches an essentially fully-hydrated state within the first 24-48 h and subsequently change very little. An intermediate partially-hydrated state is clearly apparent for AlPO-53(B), but we have not yet identified its nature.

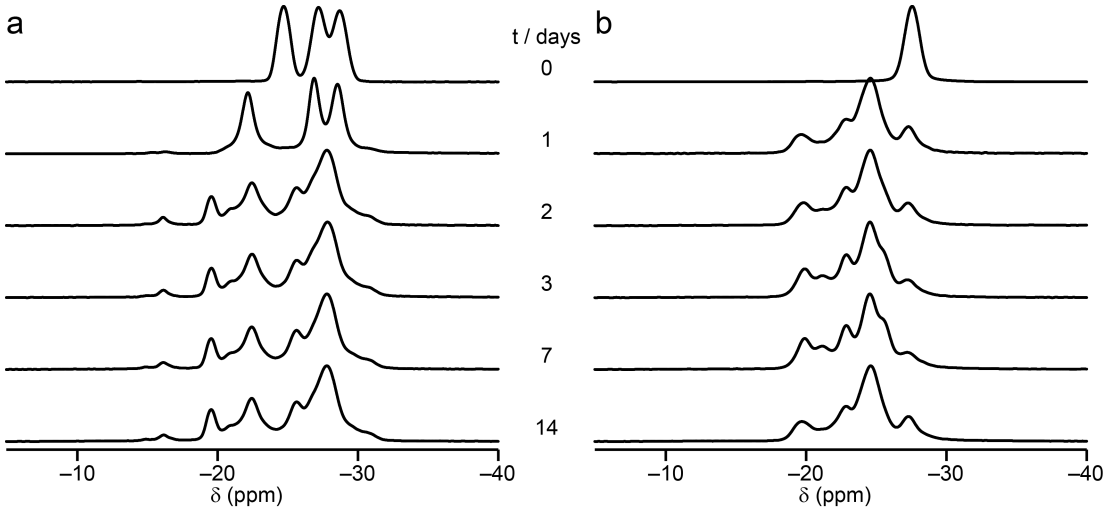

Figure S2 ^{31}P (14.1 T, 12.5 kHz MAS) NMR spectra of calcined AlPOs with (a) AEN framework type (AlPO-53(B)) and (b) CHA framework type (AlPO-34) exposed to ambient conditions for the time indicated.

S3. ^{1}H DQMAS NMR Spectra of JDF-2 and AlPO-53(A)

Assignment of the ^{1}H NMR spectra of JDF-2 and AlPO-53(A), shown in Figure 3, was confirmed by ^{1}H DQMAS spectra, shown in Figure S2. For JDF-2, the spectrum contains only one pair of off-diagonal resonances, with shifts of (3.0, 9.1) and (6.1, 9.1) ppm, confirming the close spatial proximity of the two H species with shifts of 3.0 and 6.1 ppm, previously assigned to C**H**$_3$ and N**H**$_3$, respectively. On-diagonal resonances are also observed at (3.0, 6.0) and (6.1, 12.2) ppm, as would be expected for both C**H**$_3$ and N**H**$_3$. The resonance at 5.3 ppm, assigned to O**H**$^-$ does not appear in the DQMAS NMR spectrum, confirming that this resonance arises from spatially isolated ^{1}H nuclei, as would be expected from the structure of JDF-2.

For AlPO-53(A), the ^{1}H DQMAS spectrum contains sets of on-and off-diagonal resonances that can be traced out to give C**H**$_3$ and N**H**$_3$ shifts of 2.8 and 6.6 ppm for one MA and 3.0 and 6.3 ppm for the other (indicated by solid red and blue lines, respectively). DQCs are also observed at (5.2, 8.0) and (2.8, 8.0) ppm, corresponding to a close C**H**$_3$-**H**O$^-$ distance. There is also a weak correlation between **H**$_2$O and N**H**$_3$ (although only one of the pair of expected DQCs is observed in each case), supporting the idea that there is a close spatial proximity between H_2O and the NH_3 groups, as discussed in the text.

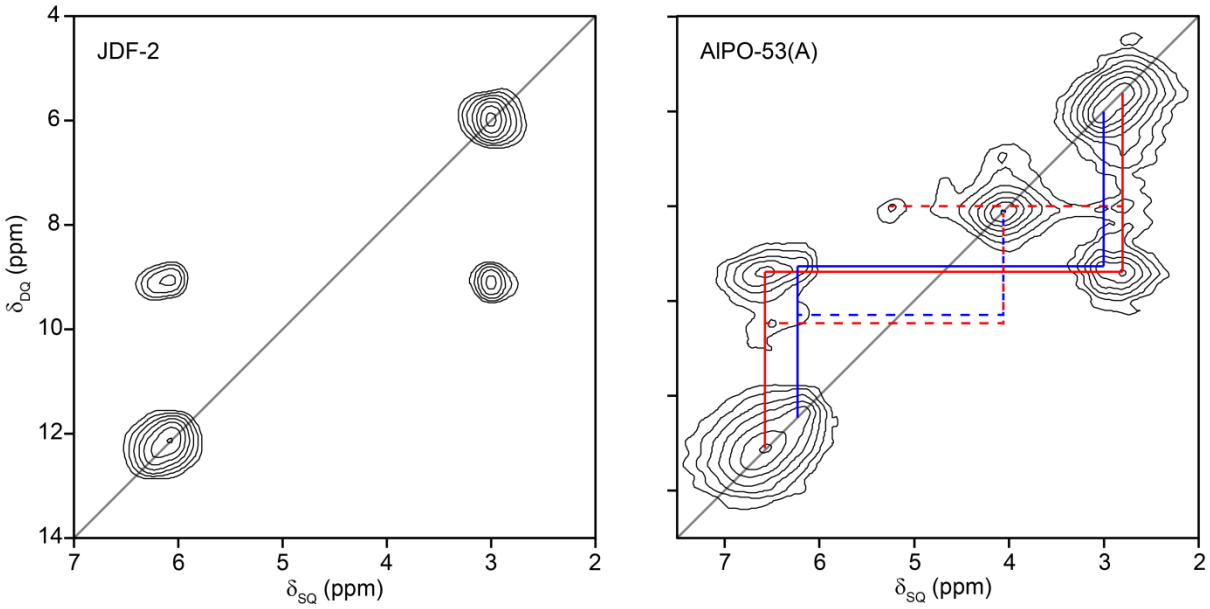

Figure S3 ^{1}H (14.1 T, 60 kHz MAS) double-quantum/single-quantum correlation spectra of JDF-2 and AlPO-53(A). In both parts, the $\delta_{DQ} = 2\delta_{SQ}$ diagonal is indicated in grey. For AlPO-53(A), sets of resonances arising from the same MAH$^+$ species are indicated with red and blue lines. C**H**$_3$-O**H** and N**H**$_3$-**H**$_2$O correlations are indicated with broken lines.

S4. ^{27}Al MQMAS NMR Spectra

^{27}Al MQMAS NMR spectra of JDF-2 and AlPO-53(A) are shown in Figure S3. The spectrum of JDF-2 contains three clear resonances with NMR parameters (given in Table 4) extracted from cross-sections of each ridge. The spectrum of AlPO-53(A) contains five clear resonances, with the NMR parameters (given in Table 4) extracted from cross sections of each ridge. As observed by Ashbrook *et al*. (2009), the resonances attributed to Al2 and Al4 are overlapped at 14.1 T.

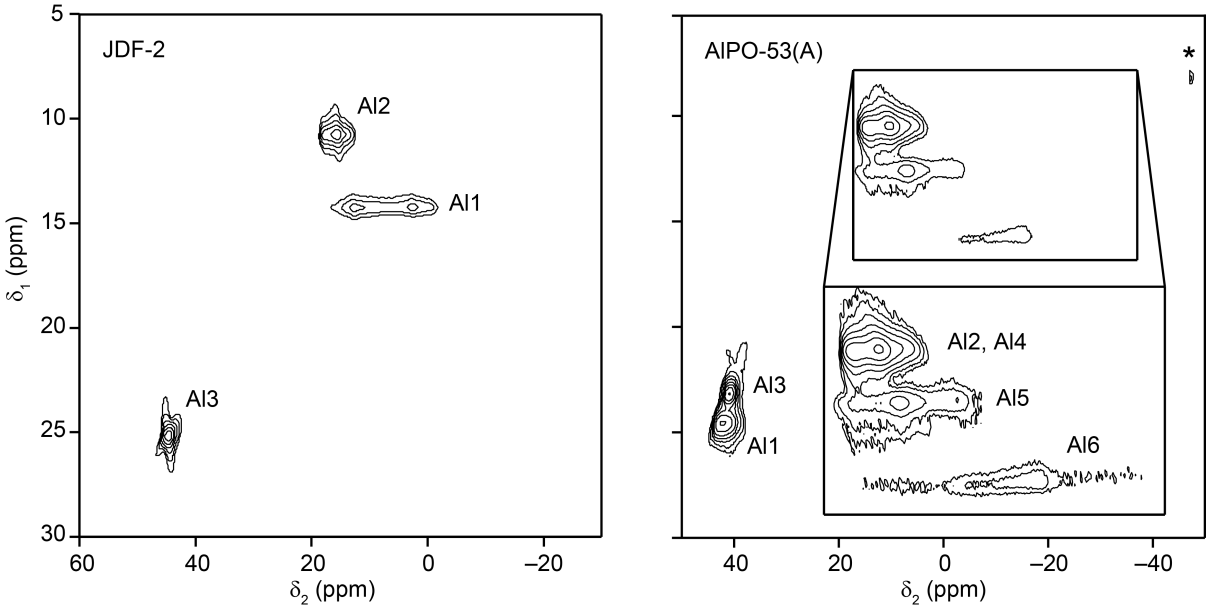

Figure S4 ^{27}Al (14.1 T, 14 kHz MQMAS) NMR spectra of JDF-2 and AlPO-53(A).

S5. Structural Models of Disorder in AlPO-53(A)

Table S1 summarises the numbering scheme used for the different models of disorder in AlPO-53(A). The input and output files for the CASTEP calculations have been uploaded separately as part of the underpinning data (see the main text for details).

Table S1 Summary of the models of JDF-2 and AlPO-53(A) considered in this work.

Model	Description	Total Energy / eV[a]
J1	Literature structure of JDF-2 (Chippindale *et al.*, 1994)	–58257.298
J2	JDF-2 with the C and N of each MAH^+ reversed	–58256.335
A1	Literature structure of AlPO-53(A) (Kirchner *et al.*, 2000)	–62037.578
A2	Literature structure of AlPO-53(A) with all water removed	–58256.446
A3	As A2 but with the C and N of each MAH^+1 and MAH^+2 reversed	–58257.290
A4	As A1 but with the C and N of each MAH^+1 and MAH^+2 reversed	–62037.612
A5	Removal of a single W1 from model A1 (before optimisation)	–61565.182
A6	Removal of a single W2 from model A1 (before optimisation)	–61565.142
A7	Removal of a single W1 from model A4 (before optimisation)	–61565.066
A8	Removal of a single W2 from model A4 (before optimisation)	–61564.687
A9	Removal of all W1 from model A1 (before optimisation)	–60147.507
A10	Removal of all W2 from model A1 (before optimisation)	–60147.320
A11	Removal of all W1 from model A4 (before optimisation)	–60146.676
A12	Removal of all W2 from model A4 (before optimisation)	–60146.536
A13	A3 containing a single W1	–58729.193
A14	A3 containing a single W2	–58729.156

a. Dispersion-corrected total energy after full geometry optimisation.

S6. Calculated ^{31}P Chemical Shifts

Figure S4 shows the calculated ^{31}P chemical shifts for the different models of AlPO-53(A) and JDF-2 discussed in the text. It can be seen that no one model is a clear match for the experimental ^{31}P NMR spectrum of AlPO-53(A). However, for JDF-2, the agreement is much better for model J1 than J2.

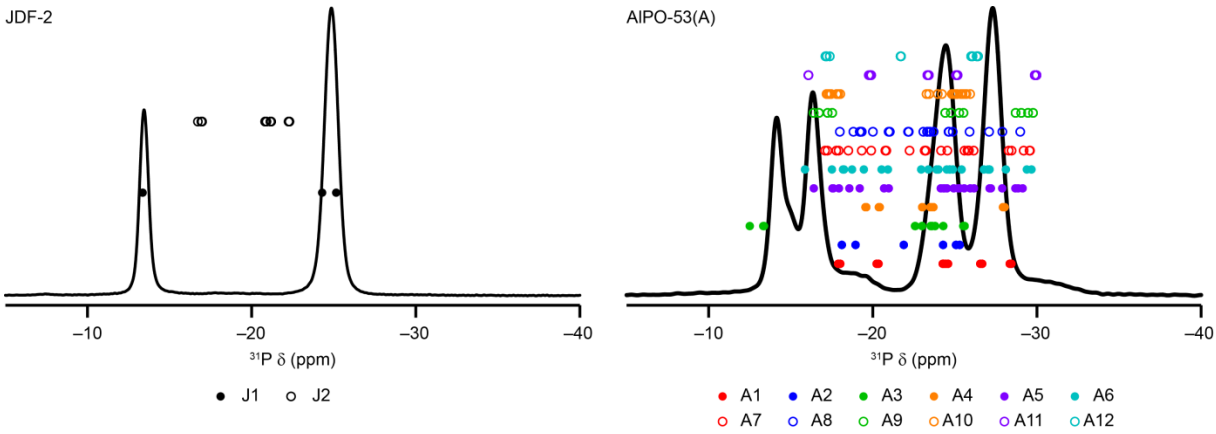

Figure S5 Experimental ^{31}P NMR spectra of AlPO-53(A) and JDF-2 overlaid with data points representing the calculated isotropic chemical shifts for the structural models discussed in the text (see Section S4 for details).